NASA SRB data

We present the analysis of the global-integrated mid-infrared emission flux of the Earth based on data derived from satellite measurements. We have studied the photometric annual, seasonal, and rotational variability of the thermal emission of the Earth to determine which properties can be inferred from the point-like signal. We are interested in the relevant conditions to retrieve the physical characteristics of the planet from the thermal light curve: geography, weather, eccentricity, axis tilt, phase angle, etc. Section 4.1 is an introduction to Earth seen as an exoplanet, the analysis of the time series, rotation rate and longitudinal light curves is presented in Section 4.2. Section 4.5 discuses the contribution of a satellite to the planetary signal and particularly the case of the Earth-Moon system and the conclusions are given in Section 4.6.

4.1 Introduction

Although the aim of numerous studies in transit spectroscopy is the characterization of terrestrial planets around M stars, in this thesis, we are focused in the characterization of an Earth analog around a G star. This case is more challenging for several reasons: G stars are less numerous than M stars, the transit probability in the habitable zone is 10 times lower than it is for M stars, the orbital period (and thus the duration between two transits) is significantly longer for G stars, and the planet-to-star contrast ratio is less favorable for secondary eclipse spectroscopy. For this matter, direct detection seems to be necessary to study Earth analogs around G stars and several instrument concepts have been proposed (Traub et al., 2006; Danchi & Lopez, 2007; Trauger & Traub, 2007; Cash et al., 2009); depending on the concept, it is either the light scattered in the visible or the infrared emission that can be detected. Then, both spectroscopy and photometry can then be used to derive

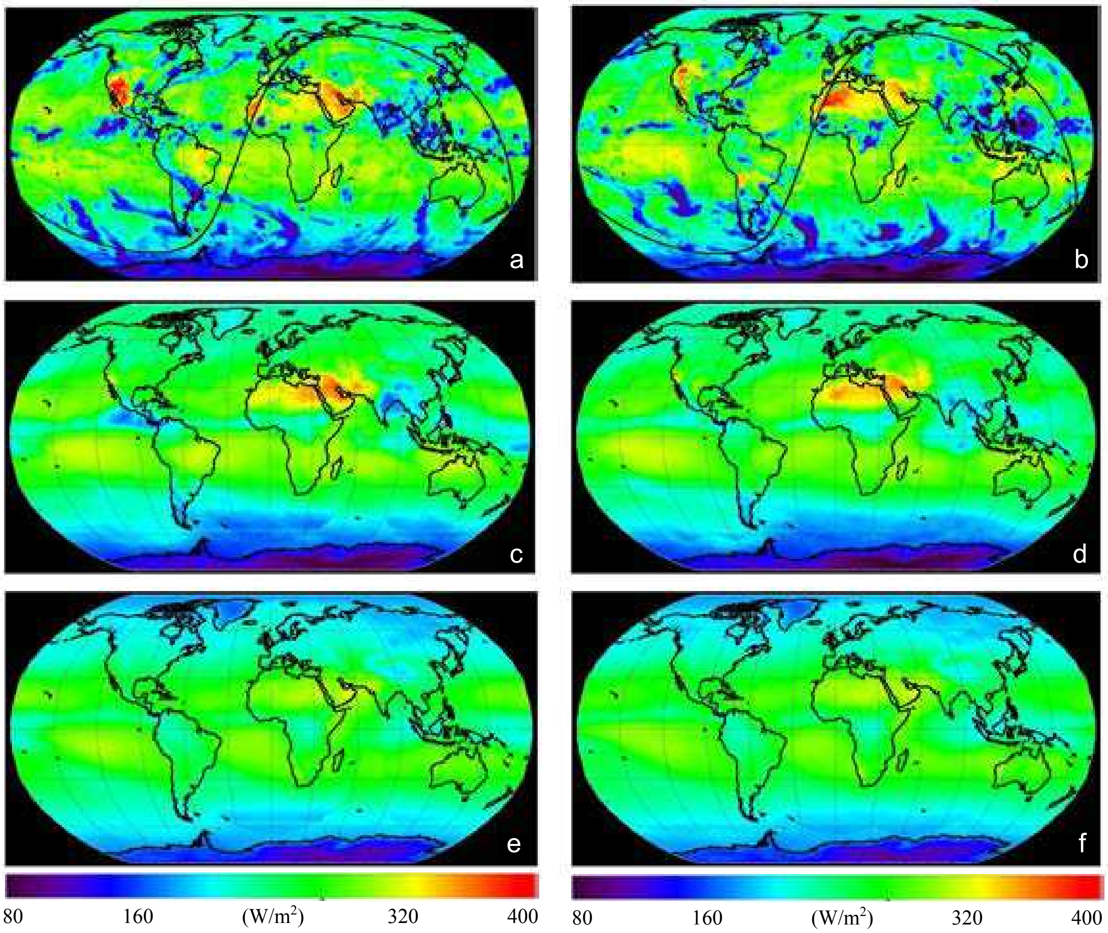

FIGURE 4.1 Maps of Earth's outgoing mid-infrared radiation. Average over the period 18:00–21:00 UT of 1987 July 1 (a) and 2001 July 1 (b) together with the subsolar point and the terminator at the mean time. At that time the brighter regions of the Earth correspond to the deserts of Sahara, Arabian Peninsula, Atacama, and Arizona. Average over the months 1987 July (c) and 2001 July (d). Average over the years 1987 (e) and 2001 (f).

some planetary properties. An important step toward these ambitious programs is to determine what level of characterization could be achieved when observing the Earth as a distant *pale infrared dot*. For instance, in the optical range, broadband photometry can potentially give us information about the albedo and the cloud cover.

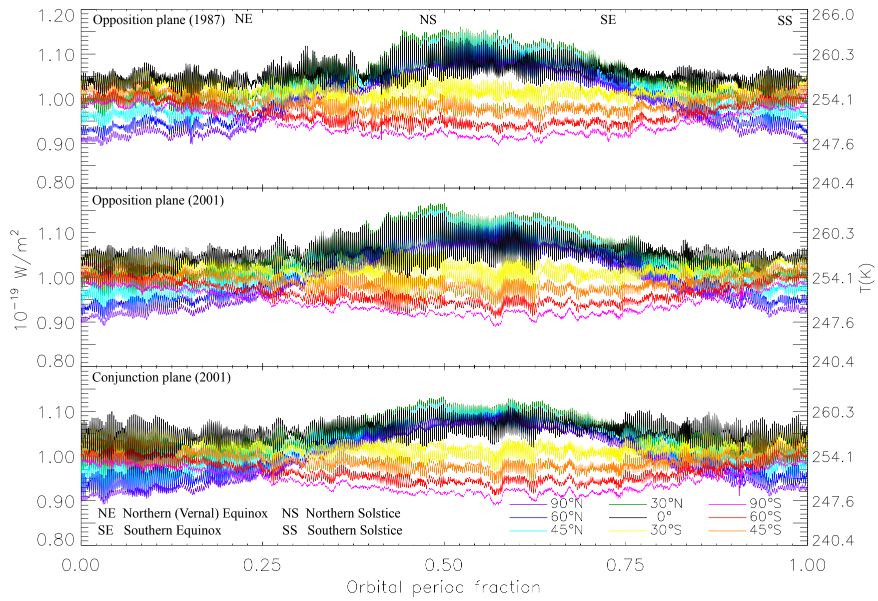

FIGURE 4.2 Time series of the mid-infrared emission flux for the two years of 1987 (top) and 2001 (middle and bottom). The sub-observer's point is represented by the latitudes 90°N, 60°N, 45°N, 30°N, 0°, 30°S, 45°S, 60°S, 90°S, and 0° longitude at the initial time (January 1, 0:00 UT) and the direction planes of opposition (O) (top and middle) and conjunction (C) (bottom).

The uneven distribution of oceans and continents enables the measurement of the 24 hr rotation period by the autocorrelation of the signal for several viewing inclination angles despite the presence of active weather (Pallé et al., 2004, 2008). Visible and near-infrared spectroscopical studies have been made by, e.g., Hearty et al. (2009), Cowan et al. (2011), Robinson et al. (2011), and Livengood et al. (2011) observing rotational and seasonal variations of the Earth spectrum and their influence on the detectability of the spectral signatures of habitability and life.

In this chapter, we provide an integrated mid-infrared (5–50 μm) photometric time series model of the Earth, with 3 hr time resolution, over a period of 22 years of available satellite data. From this geographically resolved data set, we derived the disk-integrated photometric signal of the Earth seen as a point-source planet. The NASA-SRB thermal emission maps of the Earth clearly show warm areas over the

Table 4.1. Photometric Variability of the Integrated Earth Mid-infrared Flux (Percentage Over the Mean Value)

Viewing Angle	Orbital Amplitude		Rotational Amplitude			
	1987	2001	Jan	Apr	Jul	Oct
90°N (N. Pole)	20	19	1	1	2	1
45°N (Mid-lat)	14	14	4(6)	4(4)	8(5)	5(5)
0° (Equator)	6	5	5(8)	5(4)	8(5)	4(5)
45°S (Mid-lat)	7	7	3(5)	3(2)	3(2)	2(3)
90°S (S. Pole)	11	10	1	1	1	1

Note. — Mean amplitude values of the orbital (seasonal) variability for the years of 1987 and 2001 and of the rotational variability over the months of 2001 January, April, July and October for (O) and (C) (in parenthesis) observers situated at different latitudes. Each value is calculated as the percentage of the average variation over the mean value. Data analysis for different years/months retrieves similar results.

deserts and cold spots over cold or humid regions of the planet (Fig. 4.1 a-b). These features are still relevant over monthly (Fig. 4.1 c-d) and annual averaged maps (Fig. 4.1 e-f). As we will see in this chapter, along with the uneven distribution of land and oceans over the planet, with a predominance of land masses in the Northern Hemisphere (NH), are the major factors that modulate the particular thermal emission of the Earth.

4.2 Time series analysis

Two examples of the annual time series of Earth's outgoing mid-infrared radiation are plotted in Figure 4.2. The high frequency variability corresponds to the emitted mid-infrared flux due to Earth's rotation superimposed to the seasonal variation during the year. It is readily observable from the figure that the amplitude of the rotational variability is larger for an observer in the equatorial plane (black) and decreases toward more poleward views (violet, magenta). On the contrary, because the obliquity of the Earth is about 23.44° and then the variation of the annual insolation is larger at higher latitudes, the amplitude of the seasonal variability increases for the polar geometries and decreases towards an equatorial view.

As it is expected, the seasonal variation of the northern latitude time series is opposite to the southern one due to the seasonal cycle of solar insolation. For observers over the Northern Hemisphere, the time series reach a maximum during the boreal summer near the beginning of August (orbital period fraction)(opf)~ 0.6). The equatorial view follows the same pattern, showing a "northern-biased" behavior of the planet. As we have explained in the previous section, this is due to the existence of large landmasses in the Northern Hemisphere that emit more infrared radiation than the oceans and make the northern summer hotter. In the time series, this effect is accentuated by the planetary view.

Table 4.1 shows the amplitude values of the seasonal variability of the globally integrated mid-infrared flux for the years of 1987 and 2001 and for five viewing geometries: 0° (Equator), 45°N, 45°S, 90°N (North Pole) and 90°S (South Pole). The amplitude is given in percentage change over the annual mean value. In order to conduct a seasonal study of the mid-infrared Earth emission, four representative months (January, April, July and October) were selected per year. For the sake of simplicity, we present in particular the results of the year 2001, however the rest of the data set give similar results. For comparison, we give the values taken by the observers placed in the opposition and in the conjunction planes (in parenthesis), because they have the same view of the planet at different local hours. We can see that the orbital amplitude variation of a northern latitude is twice the value of the southern equivalent latitude. The seasonal variability dominates the signal in most latitudes except for the equator, where seasonal and rotational variability are similar. It is notable that whereas the mean temperature varies with the season, the rotational variability depends strongly on the local hour (Section 2.2). This effect can be seen in the black graphs of the two bottom charts of Figure 4.2, each graph correspond to two observers at the equator plane at opposite sides of the planet. The observer placed at opposition the 1st of January (opf=0) sees the planet at midnight, whereas the observer placed at conjunction sees the planet at midday. In summer (opf$\sim$ 0.5), the planetary view is the opposite, the observer at opposition sees the planet at midday and the observer at conjunction sees the planet at midnight. Mid-latitude and equatorial viewing geometries show a pronounced and synchronized rotational variability (up to 8% in change), whereas the polar light curves present almost no variations.

4.3 Periodicities

The duration of the statistically significant peaks in the autocorrelated time series can give us an estimation of the lifetime of the cloud structures, typically of around one week for Earth clouds (Pallé et al., 2008). In the outgoing mid-infrared radiation flux, a 24 hr rotation period is clearly shown, a value close to the true rotation period. This rotational signature has two origins. First, some large regions exhibit systematically high or low brightness temperatures. This is the case for Indonesian and Sahara areas, as the former is one of the most humid and cloudy regions on the planet, whereas the latter is warmer and drier than Earth's average. Therefore, the two regions appear as fixed cold and hot features respectively, even on averaged outgoing flux maps, as we can see in Figure 4.1(c) and (d) where the TOA emission is averaged over a month and in Figure 4.1(e) and (f) where it is averaged over a year. A smaller effect comes from the diurnal cycle (the change of brightness temperature between day and night in a region), which is negligible in most locations, because of humidity, clouds, or ocean thermal inertia, but noticeable in some dry continental areas as we discuss in the next section. In fact, it is the diurnal cycle of the dry

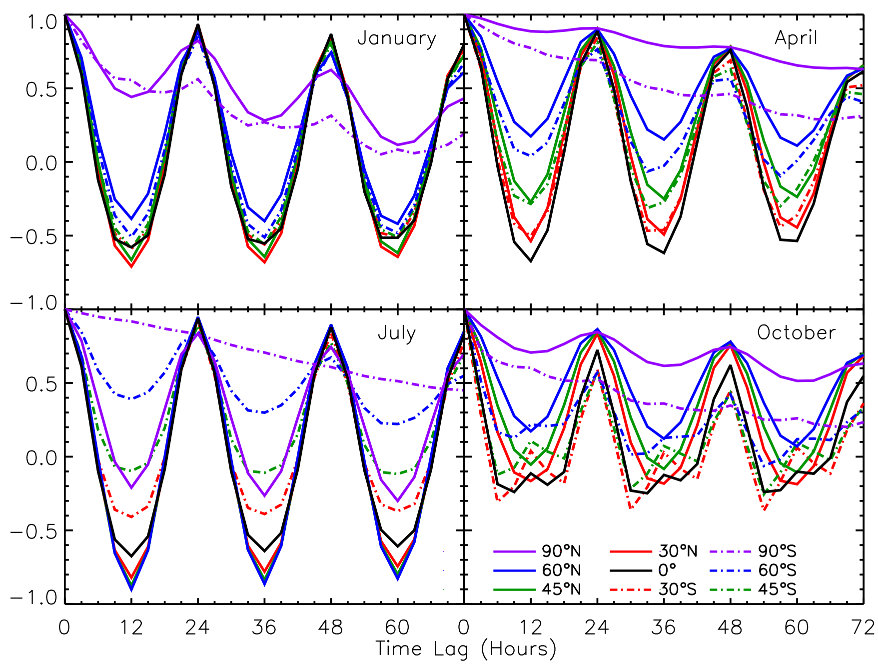

Figure 4.3 Autocorrelation functions of the mid-infrared emission flux from Earth. 2001 January, April, July, and October for the latitudes 90°N, 60°N, 45°N, 30°N, 0°, 30°S, 45°S, 60°S and 90°S.

lands, which makes possible the detection of the rotation period for the case of the North-polar view during the more stable seasons (winter and summer), as it is shown in Section 2.2. Although it is always the same fraction of the planet (the whole northern hemisphere) in the field of view, the change in temperature along the day in the dry continental areas causes the rotational modulation, as it is shown in Figure 4.3 (violet solid line). However, an observer looking at the South Pole does not detect a significant rotational variability, Figure 4.3 (violet dash-dotted line), not even for the austral summer when the effect of clouds would be minimized. In the Southern Hemisphere, the distribution of land is largely dominated by oceans whose high thermal inertia make diurnal temperature variability negligible.

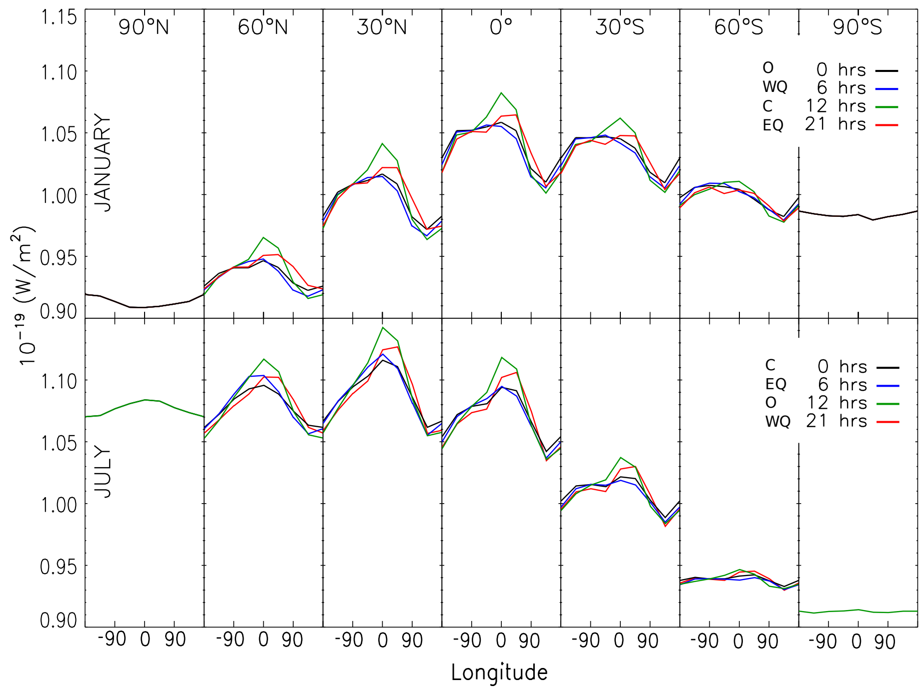

FIGURE 4.4 Rotational light curves of the mid-infrared radiation emitted from the Earth. 2001 January (top row) and July (bottom row) for the latitudes 90°N, 60°N, 30°N, 0°, 30°S, 60°S, and 90°S latitudes, the colors correspond to local hours, 0 hr (black), 6 hr (blue), 12 hr (green) and 18 hr (red) and the direction planes of opposition (O), conjunction (C), western quadrature (WQ) and eastern quadrature (EQ).

4.4 Average Rotation Light Curves

Once the rotation period is identified, the observer can produce a typical rotation light curve by folding the time series obtained during weeks or months over the rotation period. This process averages out random cloud variability. It is clearly seen on the maps of Figures 4.1(c)–(f), where the clouds disappear for longer average times whereas the strongest features mentioned on the previous section prevail. Then the observer can plot this average rotation light curve as a function of an arbitrary longitude (in our case the longitude that we have chosen is the conventional geographic longitude for commodity). The shape of the light curve can then reveal

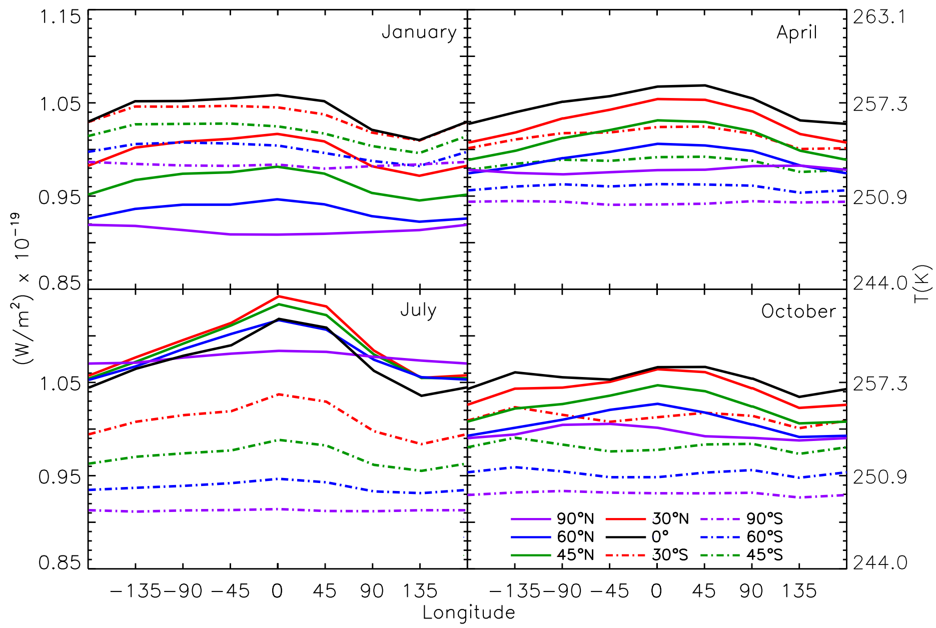

Figure 4.5 Rotation light curves of the mid-infrared radiation emitted from the Earth. For the months of 2001 January, April, July and October, 0° longitude and latitudes: 90°N, 60°N, 45°N, 30°N, 0°, 30°S, 45°S, 60°S, and 90°S.

brighter/fainter areas distributed in longitude. For instance, observers over a latitude of 30°N would note that the brightest and faintest point of the light curve occur when the longitude 0° (Sahara) or 135° (Indonesia) are respectively centered on his view. The results are represented in Figure 4.4 and Figure 4.5.

Figure 4.4 represents the rotational variability respect to the local hour for several latitudes (in column) at the months of January (top row) and July (bottom row). Each graph corresponds to four observers initially placed at the four astronomical longitudes (meridional planes) O, C, WQ, EQ, previously defined, at the same latitude (at the top of each chart). Each of these four meridional planes correspond to a certain local hour that changes with the orbital movement of the planet. With this information, we can compare the temperature evolution for a given planetary region along the day (diurnal variability). The figure shows that the longitudes that reach the maximum of temperature, have also the largest variation along the day; whereas the

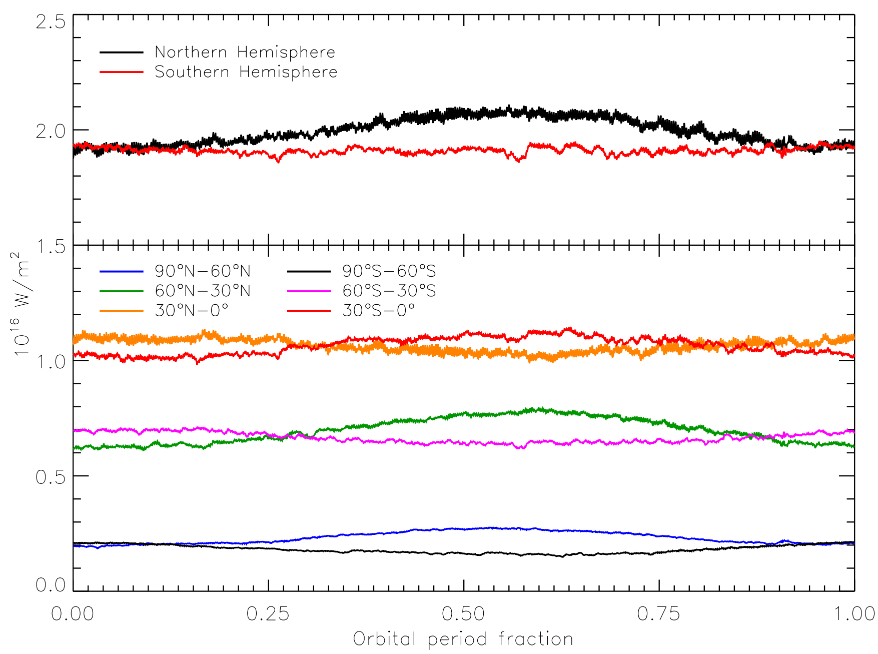

FIGURE 4.6 TOA–LW infrared emission flux of the Northern and Southern hemispheres. Total emission (top) of the Northern Hemisphere (black) and Southern Hemisphere (red). Latitude bands (bottom) of 90°N–60°N (blue), 60°N–30°N (green), 30°N–0° (orange), 90°S–60°S (black), 60°S–30°S (magenta) and 30°S–0° (red).

longitudes where the minimum is attained, show a little variation. For the cases where the observers are placed over the poles, the planetary view does not change with time so the local hour of the graph is taken just as reference of the observation time (Section 2.1). For the North Polar view, not only during summer but also during winter, the minima occurs when it is 0 UT (0 hr at 0° longitude or 12 hr at 180° longitude) and the maxima when it is 12 UT (0 hr at 180° longitude or 12 hr at 0° longitude), which illustrates the diurnal cycle effect previously mentioned. These hours coincide respectively to midnight and midday in the Sahara desert. The greatest influence of this region is noticed at the chart of 30°N latitude when the Sahara-Arabian region (15°W-50°E) is in the center of the planetary disk. The rotational amplitude is also influenced by the seasonal cycle, as we can see in the flux difference between January and July. Either in summer or winter the diurnal variability reaches the 2% at low

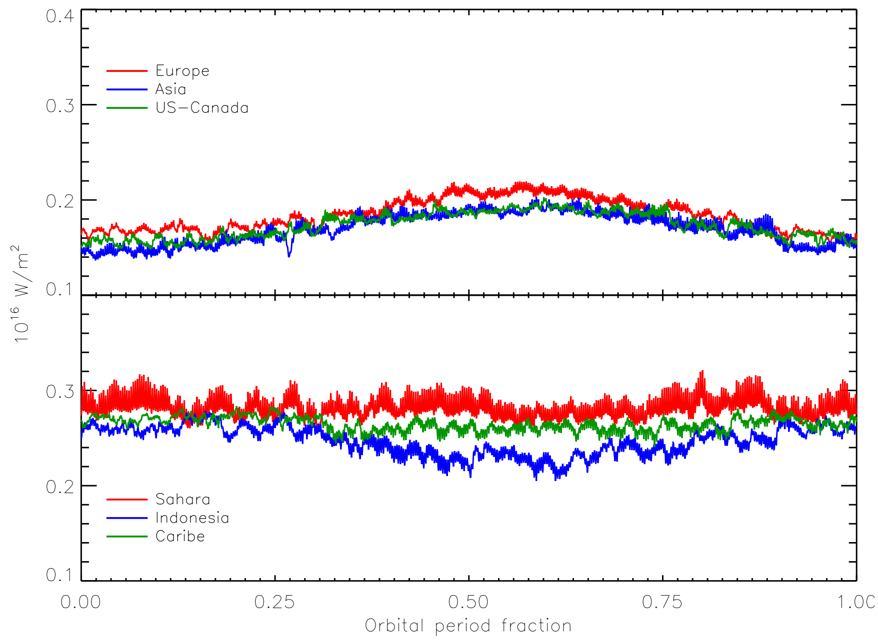

Figure 4.7 TOA–LW infrared emission flux of some continental regions in the Northern Hemisphere. In the 60°N–30°N latitude band (top): Europe (red), Asia (blue), and US-Canada (green). In the 30°N–0° latitude band (bottom), Sahara-Arabian (red), Indonesian (blue), and Caribbean-Mexico area (green).

latitudes, although the main contribution to the flux is due to the solar insolation along the year (seasonal cycle) and to the rotation variability. For Polar views, the amplitude is only due to the diurnal variability.

Figure 4.5 represents the rotational variability for observers placed at 0° longitude and different latitudes. It is important to note the temperature evolution with time for each geometry, implying a seasonal behavior. The equator shows a warm stable temperature during the year, whereas the summers of each hemisphere differ being the northern summer hotter, as it is shown in Figure 4.4. The maximum and minimum regions do not change with the seasons, except for April and October when the presence of the clouds can mask the signal.

In order to check the possible source of the diurnal variation on the Northern Hemisphere, we have made a further analysis of the emitted flux by geographic

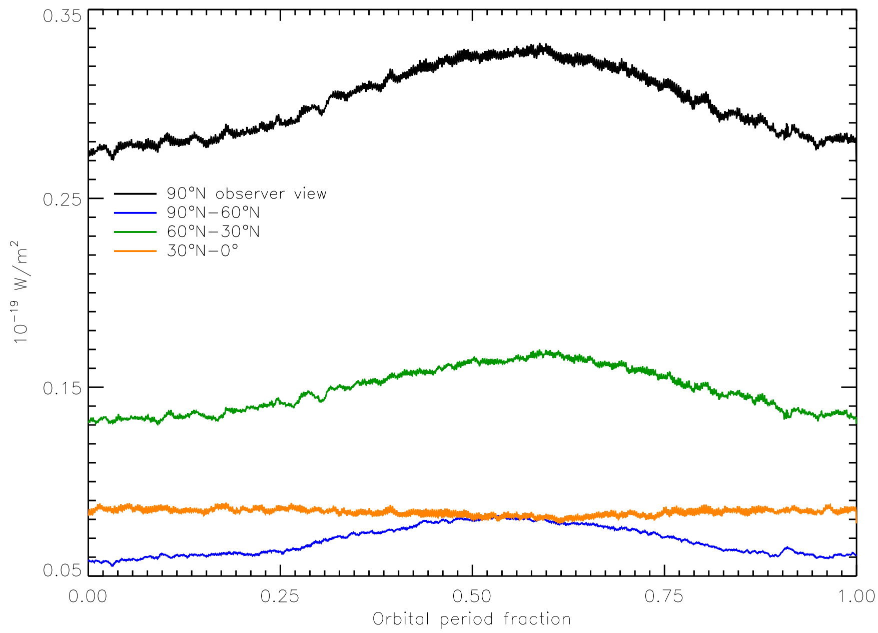

FIGURE 4.8 Time series for a North Polar observer (black) and the contribution of each latitude band to the signal. 90°N–60°N latitude band (blue), 60°N–30°N (green) and 30°N–0° (orange).

latitude bands. Figure 4.6 shows the mid-infrared emission of the Earth along one orbital period. Each hemisphere is divided in three latitude bands of flux: 90°N–60°N (blue), 60°N–30°N (green), 30°N–0° (orange), 90°S–60°S (black), 60°S–30°S (magenta), 30°S–0° (red). We can see that the Northern Hemisphere exhibits a larger seasonal variation than the Southern Hemisphere and this variation is more important for mid-latitudes. As it was previously mentioned, the greater diurnal variability comes from the latitudinal band 30°N–0°, also in this band, there is a decrease in flux during summer. This is due to the migration of the Intertropical Convergence Zone to these latitudes, which produces large bands of humidity and clouds with low brightness temperatures. As expected, we can observe that the Southern Hemisphere is in general colder than the North Hemisphere, and this difference is particularly remarkable between the South and the North poles.

For the identification of the region that produces the largest variability, we have analyzed the emission of six regions of the planet (Figure 4.7). The chosen regions have an area of 30°×60° latitude–longitude, then fluxes from the same latitude band can be compared. For the 60°N–30°N band we have chosen three regions centered in Europe (red), Asia (blue) and US-Canada (green). For the 30°N–0° band the regions are centered in the Sahara-Arabian deserts (red), Indonesia (blue), and the Caribbean-Mexico area (green). As expected, the regions in the same latitude band have similar seasonal variabilities but the Sahara region emits more infrared flux and has greater diurnal variability.

However, the emission received by the observer changes with the view of the planet. In the most favorable case, an observer placed over the North Pole, the Sahara desert lies near the limb of the planetary disk and its influence on the signal is lessened by the perspective. In Figure 4.8, we can see the contribution of high- (blue), mid- (orange), and low- (green) latitudes to the signal received by an observer placed over the North Pole (black), a case in which the rotational variability is only produced by the diurnal cycle, as the planet presents the same face along its rotation. Then, the contribution to the diurnal variability of the signal is mainly due to low and mid-latitudes. Comparing Fig. 4.4, Fig. 4.5, and Fig. 4.6 with the signal received (Figure 4.2), we conclude that although there is a small difference between day and night produced by the warm areas, the signal is dominated by the seasonal behavior.

4.4.1 Phase Variation

While Earth's visible flux received by a remote observer is modulated by the changing phase of the planet, the Earth does not present significant phases when the integrated infrared flux is observed: the emission from the nightside contributes nearly as much as the emission from the dayside (Selsis, 2004).

As we have previously explained, the diurnal variability (1%-2%) is in general lower than the rotational (1%-8%) and the seasonal variability (5%-20%). This is shown in Figure 4.2 (middle and bottom), which represent opposite observers and then opposite visible phases of the planet. An observer at opposition (O) sees the winter midnight, the observer at conjunction (C) sees the winter noon which shows a similar average temperature but a larger rotational variation. Figure 4.4 shows this difference between observers at O, C, WQ and EQ. The effect is amplified for warm areas at low latitudes, as the Sahara desert, as they have the larger contribution to the signal and it becomes more important for observers also at low latitudes, as the area pass by the center of the planetary disk. The equatorial observers of Fig. 4.2 (black) are represented by the graphs at 0 hr and 12 hrs at the central chart (0°), although we can see the difference of phase angle in the signal, the rotational and seasonal contributions dominate. Continental surfaces and the boundary layer above them (roughly the first 1500 m of the atmosphere) experience a drop of temperature between the day and night. This diurnal cycle is insignificant above the ocean (due to the high thermal inertia of water), hence over $\sim 70\%$ of the Earth surface. Day–night brightness temperature variations affect the outgoing thermal emission only in the 8–12 μm atmospheric window and above dry continents. This happens either over very cold regions which in this case do not contribute much to the global emission, or over deserts which represent a small fraction of the Earth surface. In addition, the diurnal cycle is much less pronounced above the boundary layer, at altitudes where most of the thermal emission is emitted to space. This is the reason why phase-correlated variations of Earth brightness temperature are negligible compared with seasonal changes. Even for the observing latitudes in the 30°N–0° range, in which the Sahara diurnal cycle appears in the modulation, the winter midday is colder than the summer midnight as it is seen in Figure 4.4.

4.5 Earth–Moon System Light Curves

We have modeled the mid-infrared flux of the Moon, with the purpose of study the combined light of a planet with a natural satellite. In the case of bodies with a negligible atmosphere, as it is the case of the Moon, the phase angle is relevant to compute the thermal emission. Due to a very low surface thermal inertia, the temperature map of the starlit hemisphere of the Moon can be calculated by assuming local radiative equilibrium at the surface (Lawson et al., 2007). When calculating the disk-integrated emission, the contribution of the dark side can be safely neglected

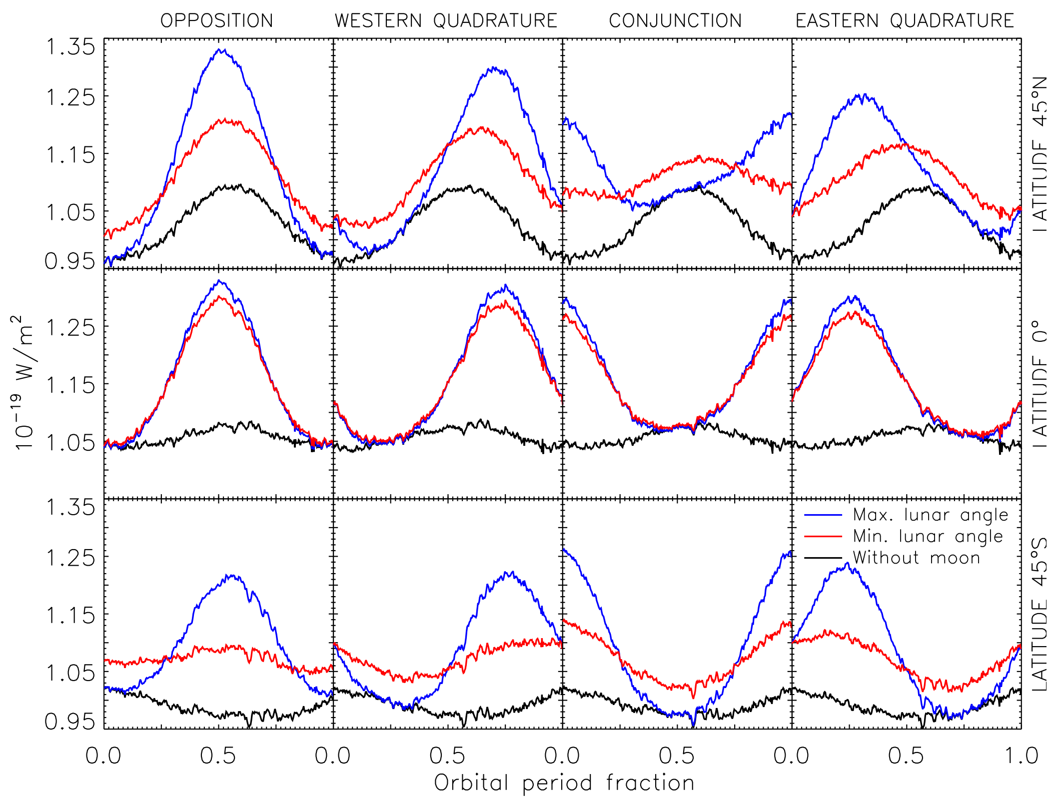

Figure 4.9 Earth–Moon mid-infrared emission light curves for one planetary orbit. 45°N (top row), Equator (second row), 45°S latitudes (bottom row), in columns the signals received by the observer's placed in opposition, western quadrature, conjunction, and eastern quadrature at the initial time. The colors correspond to the Earth (black) and Earth–Moon system, with lowest (red) and highest (blue) inclination angles of the Moon's orbit according to the observer's geometry (the possible orbits are comprehended between the two).

due to the high temperature difference. Thus, the flux received depends only on the phase of the Moon as seen by the distant observer. The amplitude of the lunar phase variations depends on the elevation of the observer above the lunar orbit, when we compute the Earth signal as a function of the latitude of the sub-observer point. As the the orbit of the Moon is not coplanar with the orbit of the Earth, a given observer latitude corresponds to a range of possible elevations above the lunar orbit. In Figure 4.9, instead of calculating this elevation consistently with the chosen observer geometry, we bracket the orbital light curve of the unresolved Earth–Moon system with the two curves obtained by adding the lunar signal for the two extreme possible elevations. As pointed by Selsis (2004) and Moskovitz et al. (2009), it presents phase variations dominated by the Moon. We note that the modulation from the satellite becomes negligible for a Moon-like satellite with 20% of the Moon radius, a $\sim 5\%$ of the radius of the planet.

The two main annual variations that modulate the IR emission from the point-like Earth–Moon system are due to the seasons of the Earth and the phases of the Moon. These modulations present a phase shift that depends on the observer geometry. For some geometries, these two modulations are coincidental. This happens if the maximum of the lunar phase corresponds to Earth's annual emission maximum, which is for instance the case for an observer looking at northern latitudes that sees the Sahara at noon in July (see Figure 4.9, the first two panels of the left column). This particular observer will see only phase-correlated variations and may attribute this variability to a day–night temperature difference and conclude that the planet has less ocean coverage and a thinner atmosphere. With such particular geometry, seasonal variations could also be mistakenly attributed to the phases in the absence of a moon, unless the lunar origin of the modulation is identified using spectroscopy (Robinson, 2011).

4.6 Summary

In this chapter, we have constructed a 3 hr resolution model of the integrated mid-infrared emission of the Earth over 20 years in the direction of a remote observer randomly located.

The seasonal modulation dominates the variation of the signal. As expected, it is larger for the polar views because the planetary obliquity causes a bigger annual insolation change for these latitudes. For equatorial views, the seasonal maximum occurs during the summer of the Northern Hemisphere, as the latter contains large continental masses whereas the Southern Hemisphere is dominated by the oceans.

The rotational variability is detectable because of the uneven distribution of oceans and continents with geographical longitude. The daily maximum of the mid-infrared flux is shown when dry large masses of land, such as the Sahara desert, are in the observer's field of view. The daily minimum appears when cloudy humid regions such as the Indonesian area is visible, as iced big zone are confined to the poles. In the polar views, the distribution of land does not change with time but the diurnal temperature variation of large continental areas affects the signal, allowing the detection of the rotational period in the North Polar case. We find that the rotational variations have an amplitude of several percent, which is comparable to that of the seasonal variations for some latitudes. It is important to remark the strong influence of the weather patterns, humidity and clouds are sometimes able to mask the 24 hr rotation period of the signal for several days at a time. However, this effect can be solved by time folding.

It is important to point out that the Earth does not exhibit a significant modulation associated with phase variation (phase curve). This is because the integrated thermal emission does not generally probe the boundary layer (first km of the atmosphere) where the diurnal cycle takes place. If unresolved, the Earth–Moon system would however present a phase variation of Lunar origin. A satellite of the size of the Moon would introduce a strong phase variability that would completely dominate over the planet's signal. This effect adds high complexity to its interpretation by photometry.

At the light of these results it seems that future infrared photometric observations of terrestrial planets can be useful in order to characterize their atmospheric and surface features. If the planet is not completely covered by clouds, as Venus is, the presence of strong surface inhomogeneities (continents) can be extracted from the daily variations. The seasonal cycle can also give estimates of the planet effective temperature, the variability in the obliquity of its orbit, and the distribution of land at larger scale. A further study with a Global Circulation Model combining Earth's emitted flux is ongoing.

PART IV.

PHOTOMETRIC VARIABILITY OF EARTH-LIKE PLANETS